AIP | Journal of Applied Physics

Finite difference method for analyzing band structure in semiconductor heterostructures without spurious solutions

Yu Jiang, Xunpeng Ma, Yun Xu, and Guofeng Song

Citation: Journal of Applied Physics **116**, 173702 (2014); doi: 10.1063/1.4899247
View online: http://dx.doi.org/10.1063/1.4899247
View Table of Contents: http://scitation.aip.org/content/aip/journal/jap/116/17?ver=pdfcov
Published by the AIP Publishing

Finite difference method for analyzing band structure in semiconductor heterostructures without spurious solutions

Yu Jiang (江宇), Xunpeng Ma (马勋鹏), Yun Xu (徐云), and Guofeng Song (宋国峰)[a)]
Institute of Semiconductors, Chinese Academy of Sciences, Beijing 100083, China

(Received 13 June 2014; accepted 13 October 2014; published online 3 November 2014)

To stably employ multiband **k·p** model for analyzing the band structure in semiconductor heterostructures without spurious solutions (SSs), the *Hermitian forward and backward difference* (HFBD) scheme for finite difference method (FDM) is presented. The HFBD is the discretization scheme that eliminates the difference instability and employs the Burt-Foreman Hermitian operator ordering without geometric asymmetry. The difference instability arises from employing *Foreman*'s strategy (FS). FS removes SSs caused by unphysical bowing in bulk dispersion curve meanwhile the HFBD is the only difference scheme that can accurately adapt for it. In comparison with other recent strategies, the proposed method in this paper is as accurate and reliable as FS, along with preserving the rapidness and simplicity of FDM. This difference scheme shows stable convergence without any SSs under variable grid size. Therefore, a wide range of experiment-determined band parameters can be applied to large-scale stable simulation with this method regardless of the SSs they originally generate. © *2014 AIP Publishing LLC*.
[http://dx.doi.org/10.1063/1.4899247]

I. INTRODUCTION

The **k·p** theory serves as an effective tool for describing band structure of bulk semiconductors.[1,2] Within the envelope-function approximation (EFA), it can be used to calculate band structure in real space.[3–36] By far it is the most popular method in simulating semiconductor heterostructures and devices like quantum well, superlattice (SL), infrared detectors, and semiconductor lasers.[4–11] Since the narrow-band-gap material system cannot be concisely simulated by the simplified single-band or two-band model,[7,13] it is essential to consider multiple bands simultaneously.[14] The multiband **k·p** method proposed by *Kane* has been widely applied.[1] The key idea is to reproduce the energy dispersion relation of multiple bands near critical points in the Brillouin zone. The Luttinger parameters are introduced into the Hamiltonian to consider the contribution of remote bands.[2] The main issues about stably employing this method are generally concerned in three aspects:

(i) The eigenvalue expression containing these fitting parameters is not always monotonic in **k**-space.[16–18] This unphysical bowing of the dispersion curve maps an identical E value to different **k** values, and the behavior of large **k** value is justified to be unnatural by causing some well-recognized numerical spurious solutions (SSs). The SSs pollute the physical solutions and severely affect the reliability of simulation.

(ii) The derivation of boundary condition and the choice of operator ordering for heterostructures within the EFA. It was shown that the real-space Hamiltonian is not necessary to be symmetric to generate real eigenvalues. Moreover, the symmetrized Hamiltonian neglects some intrinsic properties of heterojunction and can even yield ambiguous results.[33,34]

(iii) The numerical procedure to solve the envelope function equations. The Fourier transform method based on the plane wave expansion[20,26] can maintain original Hamiltonian with finite truncation number to avoid SSs. However, the truncation number is limited to the accuracy for calculating complex heterostructures.[35] Finite element method based on discretization is able to handle circumstances under high-order quantization, but the calculation velocity is limited by integral procedure.[21,24] Among present numerical methods, the finite difference method (FDM) is favorable and widely employed because of its simplicity and rapidness.[7,13,14,21,27–30]

The problem of SSs is widely investigated thanks to the fundamental significance, and a lot of strategies emerged to remove it.[10,14,19–26] A mature strategy to eliminate SSs should not change the experiment-determined effective mass near the Γ point, meanwhile it should be compatible with the already-selected numerical method. Methods omitting the correction term of remote band or only changing parameters to avoid SSs cannot provide good fit to original E–**k** relation.[10,19] It will be a well fit after adding the additional second-order terms to cancel the unphysical bowing, but there will be a misaligned combination of solutions of different orders (It will be discussed later).[14] Additional third-order terms will introduce an even better fit but require the treatment of the high-order derivative.[20] The symmetry-adapted finite element (SAFE) method needs to adjust shape functions, which is not compatible with FDM.[21] *Foreman*'s strategy (FS) provides a self-consistent modification of the Hamiltonian and the parameters.[22] This method accurately fits the original E-**k** relation near the Γ point and has been rigorously validated through deriving from basis.[23]

[a)]E-mail: sgf@semi.ac.cn

When FS is applied, the momentum terms is material-dependent and the envelope function of conduction band (CB) is no longer continuous at abrupt interfaces.[3,22] Although the abrupt envelope function is justified to be physically equivalent to the continuous one,[31] the boundary condition of each band should be specially treated. To correctly treat the boundary condition, new basis functions[23] and interface matrix[33] are developed to derive the proper operator ordering for heterostructures. These derivations support the earlier work by *Burt*, which had derived the envelope function equation for heterostructures with the Hermitian first-order operator ordering.[3] The Hermitian operator ordering is justified to satisfy physical situation in heterostructures and simultaneously ensures numerical stability by recent reports.[18,21,24–26,30–32] It is also the only operator ordering that yields mathematically self-consistent Hamiltonian for abrupt envelope functions.[22] However, in FDM, the first-order operators are customarily symmetrized to keep the Hamiltonian symmetric,[12,27] because the simplest way is to apply symmetric centered difference (SCD) to the first-order term. The change of grid size will introduce numerical instability, which becomes another source of SSs besides unphysical bowing, fails even badly when applied to FS.[19,21,30] Symmetric forward and backward difference (SFBD)[27] tends to break the geometric symmetry.[21,30] The complexity of the staggered-grid FDM[30] makes the connection path between grids sophisticated.[21]

In this paper, a difference scheme for applying FDM to FS is presented, namely a *Hermitian forward and backward difference* (HFBD) scheme. We focus on the uniformity across the whole secular equation. To establish this uniformity, the Hermitian operator ordering is employed, and the forward and backward difference is derived *accordingly* and applied to unify the calculation of each grid. The HFBD is the accurate difference approach that conforms to *Foreman*'s derivation since it has the same quadratic equation form, which also shows reliability without the failure of bowing down like SCD.[19] This work eliminates the threat from the instability of FDM and validates a wide range of presented parameters, meanwhile still maintains the simple, straightforward and rapid features of FDM.

II. THEORY AND METHOD

The partial differential equation (PDE) form of the Schrödinger equation which describes the fluctuation of electrons in real-space is written as,

$$\left(-\frac{\hbar^2}{2m}\nabla^2 + U - E\right)\psi = 0, \tag{1}$$

where the kinetic term, which originates from $\hbar^2\mathbf{k}^2/2m$, forms a Hamiltonian together with the potential term (U). The Hamiltonian becomes a Hermitian matrix when more bands are taken into account. In the eight-band $\mathbf{k}\cdot\mathbf{p}$ model, the 8×8 matrix contains two S-like CB and six P-like valence bands (VBs), which are, respectively, the light hole band (LH), heavy hole band (HH), and the split-off hole band (SO), with different spin orientation by using the set of Bloch basis functions,

$$\begin{aligned}
u_1 &= u^S_{1/2,1/2} = |S\uparrow\rangle,\\
u_2 &= u^S_{1/2,-1/2} = |iS\downarrow\rangle,\\
u_3 &= u^P_{3/2,3/2} = -\frac{1}{\sqrt{2}}|(X+iY)\uparrow\rangle,\\
u_4 &= u^P_{3/2,1/2} = \frac{i}{\sqrt{6}}|(X+iY)\downarrow -2Z\uparrow\rangle,\\
u_5 &= u^P_{3/2,-1/2} = \frac{i}{\sqrt{6}}|(X+iY)\uparrow +2Z\downarrow\rangle,\\
u_6 &= u^P_{3/2,-3/2} = -\frac{1}{\sqrt{2}}|(X-iY)\downarrow\rangle,\\
u_7 &= u^P_{1/2,1/2} = \frac{1}{\sqrt{3}}|(X+iY)\downarrow +Z\uparrow\rangle,
\end{aligned}$$

and

$$u_8 = u^P_{1/2,-1/2} = \frac{-i}{\sqrt{3}}|(X-iY)\downarrow -Z\uparrow\rangle, \tag{2}$$

and the full form of the eight-band Kane Hamiltonian that describes bulk material E-$\mathbf{k}$ relation is written as

$$\mathbf{H}_{bulk}(\mathbf{k}) = \begin{bmatrix}
C & 0 & i\sqrt{3}S & \sqrt{2}T & iS^* & 0 & iT & \sqrt{2}S^*\\
 & C & 0 & iS & \sqrt{2}T & i\sqrt{3}S^* & \sqrt{2}S & iT\\
 & & W+Q & iB & -G & 0 & -\sqrt{1/2}B & i\sqrt{2}G\\
 & & & W-Q & 0 & G & i\sqrt{2}Q & -\sqrt{3/2}B\\
 & & & & W-Q & -iB & -i\sqrt{3/2}B^* & -i\sqrt{2}Q\\
 & & & & & W+Q & i\sqrt{2}G & -\sqrt{1/2}B^*\\
 & & & & & & W-\Delta & 0\\
H.c. & & & & & & & W-\Delta
\end{bmatrix}, \tag{3}$$

where

$$C = E_C + \frac{m_0}{m_c'}\frac{\hbar^2}{2m_0}\left(k_x^2 + k_y^2 + k_z^2\right),$$
$$W = E_V - \gamma_1\frac{\hbar^2}{2m_0}\left(k_x^2 + k_y^2 + k_z^2\right),$$
$$Q = -\gamma_2\frac{\hbar^2}{2m_0}\left(k_x^2 + k_y^2 - 2k_z^2\right),$$
$$G = \sqrt{3}\gamma_2\frac{\hbar^2}{2m_0}\left(k_x^2 - k_y^2\right) - i2\sqrt{3}\gamma_3\frac{\hbar^2}{2m_0}k_xk_y,$$
$$B = 2\sqrt{3}\gamma_3\frac{\hbar^2}{2m_0}(k_x - ik_y)k_z,$$
$$T = \sqrt{1/3}Pk_z,$$

and

$$S = \sqrt{1/6}P(k_x + ik_y).$$

The lower triangle part of Eq. (3) is constructed by Hermitian conjugation (*H.c.*) operation. Here, $\mathbf{k} = (k_x, k_y, k_z)$ is the wave vector, E_C and E_V are the band edge for CB and VBs, respectively, $E_g = E_C - E_V$ is the band gap, Δ_{SO} denotes the spin-orbit split-off energy, m_0 is the free-electron mass, P is the interband momentum matrix element, and $E_P = 2m_0P^2/\hbar^2$ to express P in terms of energy unit. m_c' is the corrected CB effective mass, which is defined by

$$\frac{m_0}{m_c^*} = \frac{m_0}{m_c'} + E_p\frac{E_g + 2\Delta_{SO}/3}{E_g\left(E_g + \Delta_{SO}\right)}. \tag{4}$$

γ_1, γ_2 and γ_3 defined by

$$\gamma_1 = \gamma_1^L - \frac{E_p}{3E_g},$$
$$\gamma_2 = \gamma_2^L - \frac{E_p}{6E_g}, \tag{5}$$
$$\gamma_3 = \gamma_3^L - \frac{E_p}{6E_g},$$

are modified Luttinger parameters, which add the CB contribution to the VB masses, where γ_1^L, γ_2^L and γ_3^L are true Luttinger parameters.

The model and parameters are provided to fit experiment results. However, the well-known unphysical bowing in bulk E-$\mathbf{k}$ relation, which leads to SSs, can be sometimes introduced by those parameters. The existence of the unphysical bowing can be estimated through assessing the monotonicity of the secular equation.[12] Equation (3) can be recast into a linear combination of terms that include all orders of $\mathbf{k}$, which is written as

$$\mathbf{H}_{bulk}(\mathbf{k}) = \mathbf{H}_i^{(2)}k_i^2 + \mathbf{H}_i^{(1)}k_i + \mathbf{H}_i^{(0)} = \begin{pmatrix} A_{11} & A_{12} & \cdots & A_{18} \\ & A_{22} & & \vdots \\ & & \ddots & \vdots \\ H.c. & & & A_{88} \end{pmatrix}, \tag{6}$$

where

$$A_{mn} = A_{mn,i}^{(2)}k_i^2 + A_{mn,i}^{(1)}k_i + A_{mn,i}^{(0)}, \quad i = x, y, z.$$

Defining $A_{CB,i} = A_{mm,i}^{(2)}$, $m = 1, 2$, the coupling terms between CB and other bands are first-order terms of k_i. If the secular equation is written in the powers of k_i^2, as Eq. (9) in Ref. 14, the coefficients of the highest-order term, which decides the monotonicity, have a common factor $A_{CB,i}$ because the CB mass is isotropic. More specifically, for four-band $\mathbf{k}\cdot\mathbf{p}$ along [001], an analytical expression to verify the existence of the non-monotonicity is further derived as

$$\alpha_3 = A_{CB,z}(\gamma_1 + 4\gamma_2)(\gamma_1 - 2\gamma_2). \tag{7}$$

It was shown that the dispersion curve is no longer monotonic when α_3 is negative.[14] FS sets $A_{CB,i} = 0$ and uses E_P to fit the isotropic effective mass of CB.[22] As a result, the instability that may introduces non-monotonicity in E-$\mathbf{k}$ relation has been eliminated. To set $A_{CB,i} = 0$, the common factor m_0/m_c' is set to zero and the expression of E_P is adjusted accordingly:

$$E_P = \frac{m_0E_g\left(E_g + \Delta_{SO}\right)}{m_c^*\left(E_g + 2\Delta_{SO}/3\right)}. \tag{8}$$

Although Eq. (8) implies the contribution from remote bands has completely cancelled the CB effective mass, FS successfully provides satisfied agreement to its parent parameters in bulk E-$\mathbf{k}$ relation near the Γ point. Subsequently, other parameters are modified through Eq. (5). A set of parameters reorganized from Ref. 15 are listed and the corresponding modifications are also shown in Table I.

To solve Eq. (6) numerically in real space using FDM, one should carefully cope with the uniformity of operator ordering and difference scheme. For clear demonstration, a relatively simple derivation starts from 1-D condition along [001], and the wave vector along the quantized direction is set to $k_z = -i\partial/\partial z$ as the differential operator to form like Eq. (1).

The operator ordering of the first-order terms should be Hermitian to achieve the uniformity and provide the self-consistency of the Hamiltonian without $A_{CB,i}$. It is also a good approximation. The interband momentum matrix element P dominates first-order terms that couple CB and VBs together. It is modified by FS and becomes material-dependent. However, Eq. (3) is designed for bulk materials and postulates that P is material-independent. The Hamiltonian for heterostructure constructed by *Burt*[3] and *Foreman*[22] has negated the symmetry and used the Hermitian operator ordering. In the upper triangle part of $\mathbf{H}_z^{(1)}$, this operator ordering is written as

$$Pk_z = P_+k_z + k_zP_-, \tag{9}$$

where

$$P_+ = p_{SZ} + \sum_r p_{rZ}[E - H_{rr}(\mathbf{r})]^{-1}H_{Sr}(\mathbf{r}), \tag{10}$$

$$P_- = \sum_r p_{Sr}[E - H_{rr}(\mathbf{r})]^{-1}H_{rZ}(\mathbf{r}), \tag{11}$$

and

TABLE I. Material parameters reorganized from Ref. 15 and its modifications by using FS. For simplicity, only parameters need to be modified are shown below. Values in brackets are recalculated from Eqs. (4), (5), and (8) where $A_{CB,i}=0$. The last column shows whether the original parameters generate monotonic E-k_z relation. Other parameters without modification can be found in Ref. 15.

Material	m_0/m_c'	E_P (eV)	γ_1	γ_2	γ_3	Monotonic E-k_z relation
InAs	−4.79 (0)	21.5 (19.118)	2.81 (4.718)	−0.09 (0.859)	0.61 (1.559)	No
GaSb	−2.25 (0)	27.0 (24.820)	2.32 (3.211)	−0.84 (−0.395)	0.46 (0.905)	Yes
AlSb	−0.12 (0)	18.7 (18.397)	2.57 (2.610)	−0.12 (−0.095)	0.66 (0.685)	No

$$p_{nn'} = -i(\hbar^2/m_0)\langle n|k_z|n'\rangle.$$

Here, $H_{nn'}(\mathbf{r})$ is the off-diagonal Hamiltonian that describes interactions between state n and state n', Bloch functions $|r\rangle$ are remote states and $p_{SZ}=P$. $H_{nn'}(\mathbf{r})$ includes two parts,

$$H_{nn'}(\mathbf{r}) = H_{nn'}^{(lc)}(\mathbf{r}) + H_{nn'}^{(nl)}(\mathbf{r}), \tag{12}$$

where $H_{nn'}^{(lc)}(\mathbf{r})$ is the local part that depends only on the bulk parameters. $H_{nn'}^{(nl)}(\mathbf{r})$ is the non-local part, which is always neglected because it is only non-zero near an interface and its influence on eigenenergy is small. For bulk material, $H_{nn'}(\mathbf{r})$ is constant and the second term on the right side of Eq. (9) vanishes. The second term of Eq. (10) is dominated by non-local terms and can be safely neglected.[3] Consequently, the symmetric operator ordering is numerically equivalent to the Hermitian operator ordering when P is invariant. If P has close values among the heterostructure, the first term of Eq. (10) is large compared with other terms in Eqs. (10) and (11). Therefore, a good approximation is to use the Hermitian operator ordering throughout the heterostructure rather than the symmetric operator ordering when the difference of P values is small. Besides, the absence of $A_{CB,i}$ makes the envelope function of CB be no longer necessarily continuous. The Hermitian operator ordering is the only ordering that maintains the mathematical self-consistency of the Hamiltonian.[22]

The second-order operators are treated as $\mathbf{H}_z^{(2)}k_z^2 \rightarrow k_z\mathbf{H}_z^{(2)}k_z$. Following the Hermitian operator ordering, the total PDE with asymmetric Hermitian Hamiltonian is

$$\left[-\frac{\partial}{\partial z}\mathbf{H}_z^{(2)}\frac{\partial}{\partial z} + \left(-i\mathbf{H}_{z,u}^{(1)}\frac{\partial}{\partial z}\right) + \left(-i\frac{\partial}{\partial z}\mathbf{H}_{z,l}^{(1)}\right) + \mathbf{H}_z^{(0)} - E\right]\boldsymbol{\psi}(z) = 0, \tag{13}$$

where $\mathbf{H}_{z,u}^{(1)}$ and $\mathbf{H}_{z,l}^{(1)}$ represent the upper and lower triangle part extracted from $\mathbf{H}_z^{(1)}$ in Eq. (6), respectively. The two-band model is shown in the same form as Eq. (13):

$$(\mathbf{H}_{2\times2}-E)\boldsymbol{\psi} = \begin{pmatrix} E_C - E & -iP\frac{\partial}{\partial z} \\ -i\frac{\partial}{\partial z}P & E_V - E + \frac{\partial}{\partial z}(-A_{VB})\frac{\partial}{\partial z} \end{pmatrix}\begin{pmatrix}\varphi_{CB}\\ \varphi_{VB}\end{pmatrix}, \tag{14}$$

where A_{VB} is the second-order term for VB and the CB's second order term (A_{CB}) is already discarded. Following Eq. (14), the secular equation is quadratic, which is written as

$$\delta E_V + \frac{\partial}{\partial z}A_{VB}\frac{\partial}{\partial z} = \frac{\partial}{\partial z}\left(\frac{-P^2}{\delta E_C}\right)\frac{\partial}{\partial z}, \tag{15}$$

where $\delta E_C = E - E_C$ and $\delta E_V = E - E_V$. In Eq. (15), the second-order term of VB is on the left side, while the second-order operator on the right side is originated from multiplying two off-diagonal first-order operators in Eq. (14) together. It is the Hermitian operator ordering that maintains the uniformity of operators of the secular equation.

Furthermore, the relevance of each grid needs to be carefully treated by choosing the proper difference scheme in numerical methods based on discretization. In general, one follows the SCD scheme to discretize the first-order terms. As the result, the two second-order operators of each side of Eq. (15) is not equivalent, which is written as

$$\frac{\partial}{\partial z}\left(\frac{\partial\boldsymbol{\psi}}{\partial z}\right)_{Left}\Big|_{z=z_j} = \frac{\boldsymbol{\psi}_{j+1} - 2\boldsymbol{\psi}_j + \boldsymbol{\psi}_{j-1}}{\Delta z^2}, \tag{16}$$

$$\frac{\partial}{\partial z}\left(\frac{\partial\boldsymbol{\psi}}{\partial z}\right)_{Right}\Big|_{z=z_j} = \frac{\left(\frac{\boldsymbol{\psi}_{j+1}-\boldsymbol{\psi}_{j-1}}{2\Delta z}\right)_{j+1} - \left(\frac{\boldsymbol{\psi}_{j+1}-\boldsymbol{\psi}_{j-1}}{2\Delta z}\right)_{j-1}}{2\Delta z} = \frac{\boldsymbol{\psi}_{j+2} - 2\boldsymbol{\psi}_j + \boldsymbol{\psi}_{j-2}}{(2\Delta z)^2}, \tag{17}$$

where j is a integer that indicates the grid index and Δz is the grid size. The disunity of Eq. (15) causes grids across the solving domain to be inconsistently calculated. The absence of $A_{CB}A_{VB}k_z^4$ decoupled odd and even grids, and then any combination of them will generate a spurious solution.[11,21,30]

To achieve the uniformity as a whole, the discretization scheme on the right side of the secular equation should forms like the left side besides the operator ordering. The standard second-order difference on the left side is

$$\frac{\partial}{\partial z}A_{VB}\frac{\partial}{\partial z}\varphi_{VB}\Big|_{z=z_j} = \frac{1}{\Delta z^2}\left[A_{VB_{j+1/2}}\varphi_{VB_{j+1}} - \left(A_{VB_{j+1/2}} + A_{VB_{j-1/2}}\right) \times \varphi_{VB_j} + A_{VB_{j-1/2}}\varphi_{VB_{j-1}}\right], \tag{18}$$

where $j\pm1/2$ stands for the intermediate points, which were customarily defined to be the mean value of the two adjacent grids (j and $j\pm1$). The discretization scheme on the right side of the secular equation should be as follows:

$$\frac{\partial}{\partial z}\left(\frac{-P^2}{\delta E_C}\right)\frac{\partial}{\partial z}\varphi_{VB}|_{z=z_j}=\frac{1}{\Delta z^2}\left[\frac{-P_{j+1/2}{}^2}{\delta E_{C_{j+1/2}}}\varphi_{VB_{j+1}}-\left(\frac{-P_{j+1/2}{}^2}{\delta E_{C_{j+1/2}}}+\frac{-P_{j-1/2}{}^2}{\delta E_{C_{j-1/2}}}\right)\varphi_{VB_j}+\frac{-P_{j-1/2}{}^2}{\delta E_{C_{j-1/2}}}\varphi_{VB_{j-1}}\right]. \quad (19)$$

Equation (15) is derived by substituting the second row of Eq. (14) into the first row. In the current work, we propose to employ forward and backward difference discriminately, and the scheme follows the Hermitian operator ordering in order to form Eq. (19), which is written as

$$\frac{\partial}{\partial z}(-iP)\varphi_{CB}|_{z=z_j}=\frac{\left(-iP_{j+1/2}\varphi_{CB_j}\right)-\left(-iP_{j-1/2}\varphi_{CB_{j-1}}\right)}{\Delta z}, \quad (20)$$

where

$$\varphi_{CB_j}=\frac{-iP}{\delta E_C}\frac{\partial}{\partial z}\varphi_{VB}\Big|_{z=z_j}=\left(\frac{-iP_{j+1/2}}{E-E_{C_{j+1/2}}}\right)\frac{\varphi_{VB_{j+1}}-\varphi_{VB_j}}{\Delta z}.$$

Obviously, Eq. (20) is exact Eq. (19). The uniformity of Eq. (15) is strictly established. The coefficients of each grid in upper and lower first-order terms are Hermitian, which consist with the operator ordering. We name it the HFBD scheme. Once the upper triangle of the matrix is established, the lower triangle is subsequently determined by the Hermitian conjugation operation, which shows the self-consistency of this HFBD scheme.

The discretized Hamiltonian of the eight-band model is directly developed from the two-band model. By setting $A_{CB,i}=0$ and employing the discretization scheme Eqs. (18)–(20), one can express the discretized Eq. (3) in a form of one-to-one correspondence, which is written as

$$\mathbf{H}_{Bulk}\rightarrow\mathbf{H}_{FDM}=\begin{pmatrix}\mathbf{A}_{11} & \mathbf{A}_{12} & \cdots & \mathbf{A}_{18}\\ & \mathbf{A}_{22} & & \vdots\\ & & \ddots & \vdots\\ H.c. & & & \mathbf{A}_{88}\end{pmatrix}, \quad (21)$$

where each of the discretized submatrix corresponds to an element in Eq. (3). Each submatrix contains coefficient of all orders,

$$\mathbf{A}_{mn}=\mathbf{A}^{(2)}_{mn,i}+\mathbf{A}^{(1)}_{mn,i}+\mathbf{A}^{(0)}_{mn,i}, \quad (22)$$

where

$$\mathbf{A}^{(2)}_{mn,i}=\frac{1}{\Delta z^2}\begin{pmatrix}-(a_0+a_1) & a_1 & 0 & \cdots & a_0^*\\ a_1 & -(a_1+a_2) & a_2 & & \vdots\\ 0 & a_2 & \ddots & \ddots & \vdots\\ \vdots & & \ddots & \ddots & a_{N-1}\\ a_N^* & \cdots & 0 & a_{N-1} & -(a_{N-1}+a_N)\end{pmatrix},$$

$$\mathbf{A}^{(1)}_{mn,i,u}=\begin{pmatrix}-b_1 & b_1 & 0 & \cdots & 0\\ 0 & -b_2 & b_2 & & \vdots\\ \vdots & & \ddots & \ddots & \vdots\\ \vdots & & & \ddots & b_{N-1}\\ b_N^* & \cdots & \cdots & 0 & -b_N\end{pmatrix},$$

$$\mathbf{A}^{(0)}_{mn,i}=\begin{pmatrix}c_1 & 0 & \cdots & 0\\ 0 & c_2 & & \vdots\\ \vdots & & \ddots & 0\\ 0 & \cdots & 0 & c_N\end{pmatrix},$$

and

$$a_j=A^{(2)}_{mn,i_{j+\frac{1}{2}}},\quad b_j=A^{(1)}_{mn,i,u_{j+\frac{1}{2}}},\quad c_j=A^{(0)}_{mn,i_j}.$$

The CB band profile is a special case of $\mathbf{H}_i^{(0)}$. It is replaced by its forward intermediate point, which is written as

$$\mathbf{A}^{(0)}_{mm,i}=\begin{pmatrix}E_{C_{1+\frac{1}{2}}} & 0 & \cdots & 0\\ 0 & E_{C_{2+\frac{1}{2}}} & & \vdots\\ \vdots & & \ddots & 0\\ 0 & \cdots & 0 & E_{C_{N+\frac{1}{2}}}\end{pmatrix}, m=1,2. \quad (23)$$

In 1-D condition along [001], $N=L/\Delta z$ and L is the total length of the simulation range along z-direction. The zeroth point and $(N+1)$th point are added intentionally to satisfy boundary conditions. The periodic boundary condition, which relates both ends by Bloch's theorem that requests $\varphi_0=e^{-iK_zd}\varphi_{N_z}$ and $\varphi_{N+1}=e^{iK_zd}\varphi_1$, can be achieved by setting $a_0^*=e^{-iK_zd}a_0$, $a_N^*=e^{-iK_zd}a_N$, and $b_N^*=e^{-iK_zd}b_N$ with d and K_z being, respectively, the periodicity and wave vector when investigating SLs. The Diriclet boundary condition needs φ_0

and φ_{N+1} to be zero. This requires that the additional zeroth point is included in $\mathbf{H}_{FDM}$. In order to make this extra point zero, the extra first column and row of $\mathbf{A}^{(2)}_{mn,z}$ and the extra first column of $\mathbf{A}^{(1)}_{mn,z,u}$ are set to be all-zero. One can simply apply parameters of the first grid to the zeroth one, since it only make this point zero and does not affect the result. All components of φ_0 should be discarded from the final solution set. Therefore, the solving domain is discretized to N sections by N intermediate points, which maintains physical length.

The lower off-diagonal submatrices are determined following Hermitian conjugation operation. Subsequently, the eigenenergy values E and the corresponding eigenvectors $\varphi_1 \sim \varphi_N$ are obtained from solving the eigenvalue of $\mathbf{H}_{FDM}$. The normalized probability density is the direct linear combination of all components in Eq. (2), which reads

$$|\Psi(\mathbf{k}_{||}, z)|^2 = \sum_{n=1}^{8} |\varphi_n(\mathbf{k}_{||}, z)|^2. \tag{24}$$

Since the CB band profile has been replaced by its forward intermediate points, the calculated $\varphi_{1,2}(\mathbf{k}_{||}, z)$ corresponds to the shifted band profile. It has a half-grid-width mismatch with other eigenvector components, which leads to disunity when applies Eq. (24). It can be easily compensated by regarding $\varphi_{1,2_{j-1/2}}(\mathbf{k}_{||}, z)$ as $\varphi_{1,2_j}(\mathbf{k}_{||}, z)$.

Following the above-mentioned operation, the geometric symmetry of the solved envelope functions is established. This method has a straightforward form by employing Eq. (21). The component of each band is seriated in Eq. (24) and can be simply retrieved.

III. RESULTS AND DISCUSSIONS

Being the first source of SSs, the unphysical bowing in bulk E-$\mathbf{k}$ relation has been widely characterized. However, SSs that arise from the instability of FDM needs to be further investigated. Currently, we set the analytical discretization expression of Bloch wave ($\psi_{j\pm1} = \exp(\pm i\Delta z\, k_z)\psi_j$),[19] where k_z runs through 0 to $\pi/\Delta z$ between adjacent grids, then a good discretization approach should reproduce the bulk E-$\mathbf{k}$ relation. The SCD of the first-order terms is written as

$$\begin{aligned} -i\mathbf{H}_z^{(1)} \frac{\partial}{\partial z}\bigg|_{z=z_j} &= \frac{-i}{2\Delta z}\mathbf{H}_z^{(1)}\psi_{j+1} + \frac{i}{2\Delta z}\mathbf{H}_z^{(1)}\psi_{j-1} \\ &= \mathbf{H}_z^{(1)} \frac{\sin(\Delta z\, k_z)}{\Delta z}\psi_j. \end{aligned} \tag{25}$$

While in HFBD, the upper and lower first-order terms are Hermitian conjugate, which is written as

$$\begin{aligned} -i\mathbf{H}_{z,u}^{(1)} \frac{\partial}{\partial z}\psi|_{z=z_j} &= \frac{-i}{\Delta z}\mathbf{H}_{z,u}^{(1)}(\psi_{j+1} - \psi_j) \\ &= \mathbf{H}_{z,u}^{(1)} \frac{1}{\Delta z}[-i\cos(\Delta z\, k_z) + \sin(\Delta z\, k_z) + i]\psi_j \\ -i\frac{\partial}{\partial z}\mathbf{H}_{z,l}^{(1)}\psi|_{z=z_j} &= \frac{-i}{\Delta z}\mathbf{H}_{z,l}^{(1)}(\psi_j - \psi_{j-1}) \\ &= \mathbf{H}_{z,l}^{(1)} \frac{1}{\Delta z}[i\cos(\Delta z\, k_z) + \sin(\Delta z\, k_z) - i]\psi_j. \end{aligned} \tag{26}$$

The E-k_z relation calculated by using parameters of InAs (Table I) is shown in Fig. (1). In bulk E-k_z relation, when k_z is near the Γ point, FS provides good fit to original curve. When k_z value becomes large, the original curve bowed down to generate SSs (denoted as k_{bulkSP} in Fig. 1), where the curve of FS is an asymptote and the unphysical bowing was removed. After discretization, trigonometric functions in Eqs. (25) and (26) determine the E-k_z relation curve of CB when $A_{\text{CB},z} = 0$. When SCD is applied, the eigenvalue of CB will be equal to E_C at $k_z = \pi/\Delta z$. The curve becomes non-monotonic and acts like unphysical bowing in bulk E-k_z relation (denoted as k_{FDMSP} in Fig. 1). Thus SCD fails to apply to FS. In contrast, the *cosine* terms in Eq. (26) make the E-k_z relation curve of HFBD clearly become an asymptote through $k_z = 0$ to $k_z = \pi/\Delta z$. As shown in Fig. 1, the HFBD is consistent with FS throughout the first Brillouin zone. Here, the CB bottom is set to be the reference energy point where $E = 0$. The grid size here is chosen to be half a monolayer (k_z is within 20.9 nm^{-1}).

The large-k behavior around CB bottom becomes unnatural and shows phenomena of oscillation.[19] Through predicting the large-k behavior, we can characterize FDM instability and discard SSs by HFBD. We start searching solutions of a 5 nm InAs quantum well confined by AlSb from the CB bottom of InAs. As the symbol-line shown in Fig. 2 (a), the application of SCD to FS leads to SSs dominated by large-k behavior localized near the CB bottom. For demonstration, very small $A_{CB,z}$ values were fixed by setting $m_0/m_c' = 0.05$ and $m_0/m_c' = 0.1$, respectively, and subject to a mathematical operation which lets the curve end up above the CB bottom (i.e., $E(k)|_{k=\pi/\Delta z} > E_C$). The localized SSs are just above the critical point where energy value starts to map two k values ($E(k)|_{k=\pi/\Delta z}$). The physical small-k solutions are retained below this critical point. For sake of clarity, only the lowest four states are exhibited due to the fact that the SSs will continue to appear above this critical point. To alleviate the problems related to SSs, some strategies by elevating this critical point has been reported.[30,36]

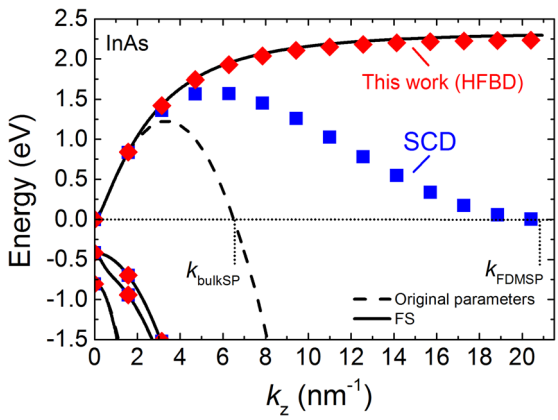

FIG. 1. The bulk E-k_z relation along z-axis with FDM approach. The dashed line represents the result of original parameters of InAs from Table I. The solid line stands for the modification of FS. The blue cubes show the SCD approach to FS. The red diamonds stand for the HFBD approach to FS.

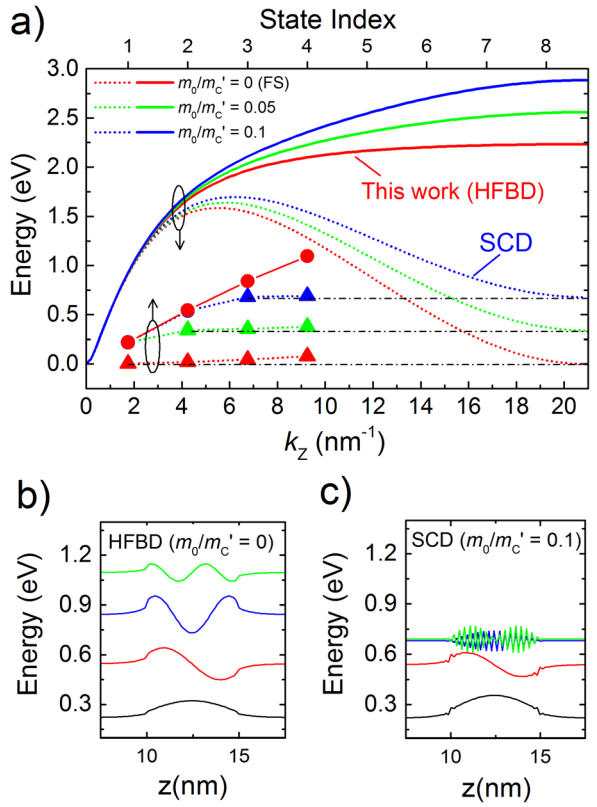

FIG. 2. (a) The large-k behavior of FDM. The lines correspond to E-k_z relation, where solid lines stand for HFBD and dotted lines stand for SCD. The symbol-lines represent energy states above CB bottom in a 5 nm InAs/AlSb quantum well, where deltas are large-k SSs and circles are physical solutions. (b) The solutions (φ_{CB}) in the quantum well correspond to the red circles in a) by HFBD with $m_0/m_c' = 0$. (c) The solutions correspond to the blue circles and deltas in (a) by SCD with $m_0/m_c' = 0.1$. The parameters are the same with Fig. 1 except the varying $A_{CB,z}$.

However, the inevitable instability of SCD results in limited selection of grid size and band parameters, whereas HFBD for FS never bows down. Therefore, SSs of FDM are generated by unstable bowing in the E-**k** relation of SCD, and they are eliminated by applying HFBD.

To emphasize the necessity of HFBD with proper choice of operator ordering, the normalized probability density of the fundamental electron state in a 5 nm InAs/GaSb quantum well was plotted. As shown in Fig. 3, the result of SCD is obtained by increasing $A_{CB,z}$ slightly. Despite of the fact that it is physical, improper operator ordering of SCD leads to poor boundary conditions, which results in oscillation around interfaces (seen from both Figs. 2(c) and 3(b)). The symmetric operator ordering in SFBD induces oscillation, although it does not bow down like SCD in E-**k** relation. Those ill boundary treatments lead to poor convergence as Table II shows, since the oscillatory behavior is related to grid size. HFBD treats the abrupt envelope function through a step between adjacent points at interfaces, and the envelope function maintains physical shape independent of grid size. Hence the alteration of the operator ordering is necessary for stable numerical procedure. The similar conclusion also had been proved elsewhere for different purposes.[24,26] Moreover, considering the first three rows to be the converged results, the deviation of eigenvalues caused by the alteration of operator ordering is within several micro electron volts, even the difference between E_P values is significant.

The uniformity throughout the heterostructure is rather important for a strategy. Within the framework of Ref.14, matrix elements of the parameters that will not generate SSs *cannot* be modified because that modification will generate SSs counteractively. The disunity caused by this discrimination affects boundary conditions at interfaces, and the

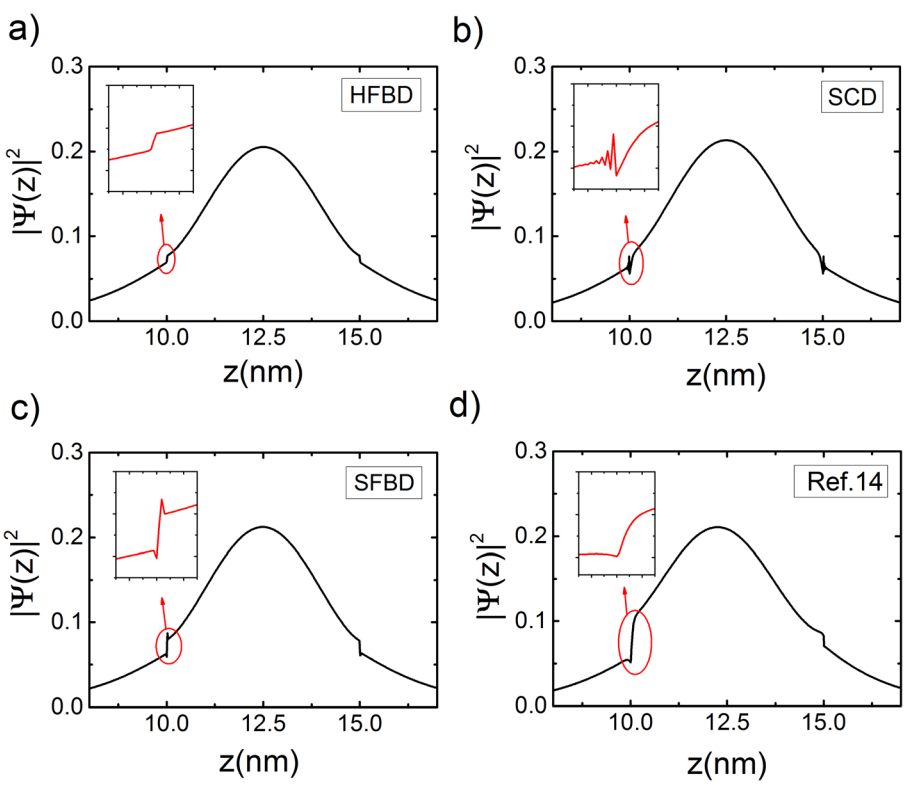

FIG. 3. The normalized probability density of the fundamental electron state in the 5 nm InAs/GaSb quantum well calculated by different strategies with parameters in Table I. Those strategies are (a) FS with HFBD, (b) FS with SCD, (c) FS with SFBD from Ref. 27 and (d) the strategy in Ref. 14. The insets are the zoom-in of their shapes at interfaces. The grid size here is 0.01 nm.

TABLE II. The eigenvalue of the fundamental electron state calculated by different strategies, as Fig. 3 shows.

Grid size(nm)	HFBD (FS) Eigenvalue (eV)	SCD (FS) Eigenvalue (eV)	SFBD (FS) Eigenvalue (eV)	Ref. 14 Eigenvalue (eV)
0.1	0.23252	0.23759	0.23818	0.24777
0.05	0.23241	0.23710	0.23755	0.24727
0.01	0.23233	0.23444	0.23387	0.24676
0.001	0.23232	0.21584[a]	0.19930[a]	0.25180[a]

[a]Applying this fine grid size, the wavefunctions are out of shape and cannot be considered as a converged result.

interfacial envelope function will fluctuate with grid size. Besides, additional second-order operators are linearly combined with first-order operators in matrix (Eq. (8) in Ref.14), causing different-order terms to be combined directly, which are, respectively, symmetric and anti-symmetric for Sturm-Liouville problem. This results in asymmetric envelope function in InAs layers (see from Fig. 3(d)). In contrast, the parameters of GaSb do not generate SSs originally, but they are still modified in this work. As a result, our method treats all involved materials uniformly and shows stable convergence, whereas other strategies show unstable eigenvalues when grid size changes (Table II). In addition, the geometric asymmetry of the strategy in Ref. 14 also severely affects applications that depend on wave functions, such as charge distribution simulation using Schrödinger-Poisson method, which was widely used in device simulation.[7,9,29] Therefore, as discussed earlier, HFBD is the only stable scheme for eliminating SSs with FS being applied.

It was shown that band dispersion relations are hybridized along the XY-plane at finite in-plane wave vector value ($|\mathbf{k}_{||}| = \sqrt{k_x^2 + k_y^2}$) in broken-gap quantum wells.[12] The parameters from Ref. 12 is applied and modified by FS for comparison. In Fig. 4, the result calculated by using SCD and original parameters is shown in dashed line, and solid lines stand for the result calculated by applying HFBD and modified parameters. The SSs appears due to the unphysical bowing introduced by original AlSb parameters. FS modification and HFBD scheme keep the nearly identical band structure and eliminate SSs. Besides the deviation in E-$\mathbf{k}$ relation, very slight deviation of eigenenergy introduced by the alteration of operator ordering is observed, since the close E_P values between InAs and GaSb in this set of parameters result in insignificant non-local terms in Eq. (9).

An interband cascade infrared photodetector (ICIP) taken from Ref. 9 is simulated by the proposed method with parameters in Table I. Fig. 5(a) shows the result of the whole structure calculated using Diriclet boundary condition and Fig. 5(b) shows the miniband of the SL absorber layers calculated using periodic boundary condition. In the InAs (2.1 nm)/GaSb (2.7 nm) SL absorber layers, the lowest CB miniband is calculated to be 0.35618 eV and the highest HH

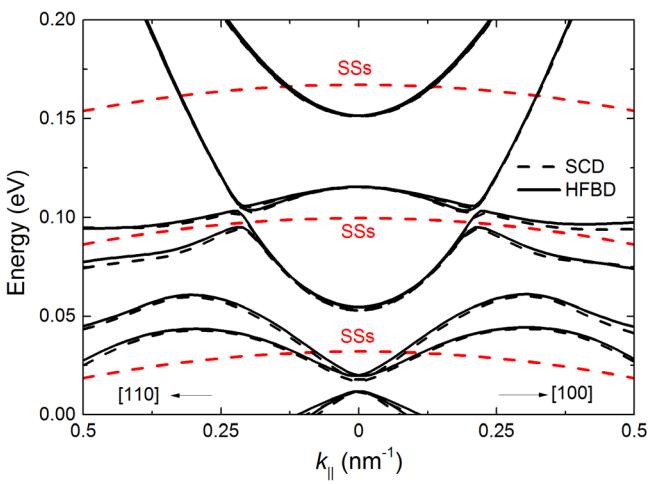

FIG. 4. The band dispersion relation along in-plane wave vector of a 10 nm/17 nm/5 nm/10 nm AlSb/InAs/GaSb/AlAs heterostructure. The solid lines represent the result solved by using HFBD scheme and modified parameters that originally taken from Ref.12. The result from original method (SCD) and parameters in Ref. 12 are reproduced in the dashed lines, where SSs are shown in red color.

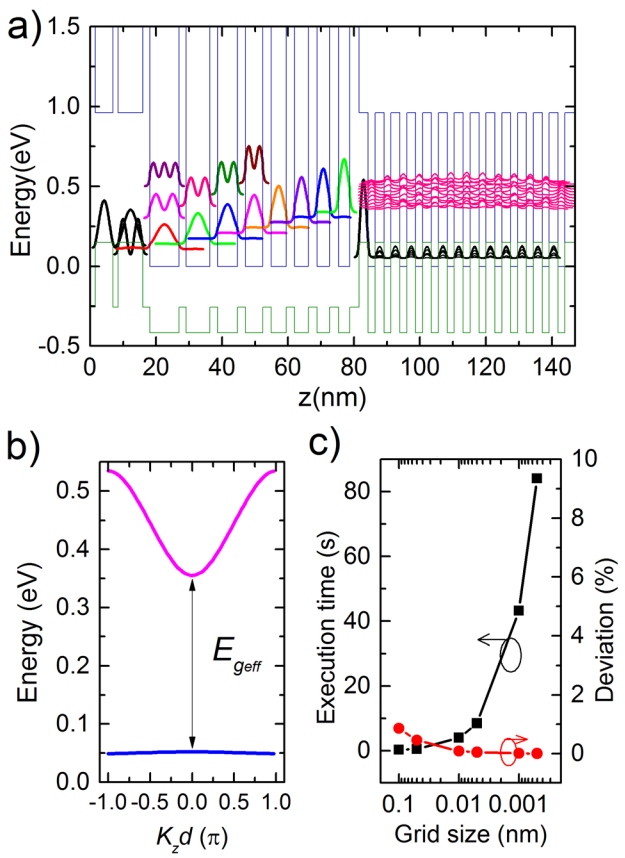

FIG. 5. (a) Simulation of an ICIP taken from Ref. 9. The SL absorber layers locate at 82 nm ~ 147 nm. The pink lines and the black lines in the SL layers stand for CB miniband and HH miniband in this type II SL, respectively. (b) The miniband of CB and HH in the SL absorber calculated using periodic boundary condition, where E_{geff} is the effective band gap in the SL structure. (c) The relationship of execution time and deviation with the grid size for the whole structure. The finest result (4.075 μm) is the reference value of the deviation.

miniband is calculated to be 0.05215 eV. The peak absorption wavelength is 4.075 μm, which conforms to the experiment results in Ref. 9 (4.0 μm). Although the set of parameters in Ref. 15 generates unphysical bowing, it has been systematically studied and provides good agreement with experiment. It will no longer compromise to avoid the unphysical bowing with the proposed method. In addition, it is worth mentioning that the execution time of the eigenvalue solver is less than 0.3 s on an ordinary desktop computer when grid size is 0.1 nm, which still maintains the deviation within 1%. The relationship of execution time and deviation with the grid size is shown in Fig. 5(c). The good convergence of this method makes it more practical for large-scale simulation.

The abrupt envelope functions at interfaces can use a fine grid size to approach by applying the non-uniform mesh FDM technology.[29] If one can set very fine meshes around interfaces, the eigenvalue will converge with even less grid amount. However, this will cause the matrix to become much more complex, and prevent the advantage of simplicity for employing FDM.

IV. CONCLUSION

In this work, a HFBD scheme for FDM is presented for stable analysis of the band structure in semiconductor heterostructure using multiband **k**·**p** method. By choosing the proper approximation, the Hermitian operator ordering and the corresponding forward and backward difference is derived to unify the calculation of each grid after eliminating the unphysical bowing in bulk E-**k** relation by *Foreman*'s strategy. The HFBD removes the difference instability and allows convergence at abrupt interfaces. In comparison with other reported methods, ours provides better uniformity and stable convergence besides the verified accuracy. The discretized matrix reflects the straightforward feature of FDM and is easy to be implemented. A type II SL is simulated by employing the proposed method and shows good agreement with the experiment result. The execution time of the eigenvalue solver for 1500 points is within 0.3 s. The improved accuracy and rapidness of our proposed method makes it prospective for stably simulating large-scale quantum system without spurious solutions.

ACKNOWLEDGMENTS

We thank Prof. Li Fu, Prof. Xuanhua Li and Prof. Min Zhang in Northwestern Polytechnical University for helpful discussions. This work was supported by the National Basic Research Program of China (973 Program) (Grant Nos. 2015CB351902, 2012CB619203, 2011CBA00608, and 2015CB932402) and the National Natural Science Foundation of China (NSFC) (Grant Nos. 61036010, 61177070, 11374295, and U1431231).

[1]E. O. Kane, J. Phys. Chem. Solids **1**, 249 (1957).
[2]J. M. Luttinger and W. Kohn, Phys. Rev. **97**, 869 (1955).
[3]M. G. Burt, J. Phys. Condens. Matter **4**, 6651 (1992).
[4]E. H. Aifer, J. G. Tischler, J. H. Warner, I. Vurgaftman, W. W. Bewley, J. R. Meyer, J. C. Kim, and L. J. Whitman, Appl. Phys. Lett. **89**, 053519 (2006).
[5]J. B. Rodriguez, E. Plis, G. Bishop, Y. D. Sharma, H. Kim, L. R. Dawson, and S. Krishna, Appl. Phys. Lett. **91**, 043514 (2007).
[6]O. Salihoglu, A. Muti, K. Kutluer, T. Tansel, R. Turan, Y. Ergun, and A. Aydinli, Appl. Phys. Lett. **101**, 073505 (2012).
[7]Y. Li, Y. Zhang, and Y. Zeng, J. Appl. Phys. **108**, 044504 (2010).
[8]I. Lo, W. C. Mitchel, R. Kaspi, S. Elhamri, and R. S. Newrock, Appl. Phys. Lett. **65**, 1024 (1994).
[9]Z. Tian, R. T. Hinkey, R. Q. Yang, D. Lubyshev, Y. Qiu, J. M. Fastenau, W. K. Liu, and M. B. Johnson, J. Appl. Phys. **111**, 024510 (2012).
[10]Y. Xiu, G. Yong-Xian, W. Qing, W. Xin, and C. Liang-Hui, Chin. Phys. B **20**, 030507 (2011).
[11]W. W. Bewley, C. L. Canedy, C. Soo Kim, M. Kim, C. D. Merritt, J. Abell, I. Vurgaftman, and J. R. Meyer, Opt. Express **20**, 3235 (2012).
[12]W. Xu, L. L. Li, H. M. Dong, G. Gumbs, and P. A. Folkes, J. Appl. Phys. **108**, 053709 (2010).
[13]X. Ma, K. Li, Z. Zhang, H. Hu, Q. Wang, X. Wei, and G. Song, J. Appl. Phys. **114**, 063101 (2013).
[14]K. I. Kolokolov, J. Li, and C. Z. Ning, Phys. Rev. B **68**, 161308 (2003).
[15]I. Vurgaftman, J. R. Meyer, and L. R. Ram-Mohan, J. Appl. Phys. **89**, 5815 (2001).
[16]M. F. H. Schuurmans and G. W. 't Hooft, Phys. Rev. B **31**, 8041 (1985).
[17]R. Winkler and U. Rössler, Phys. Rev. B **48**, 8918 (1993).
[18]A. T. Meney, B. Gonul, and E. P. O'Reilly, Phys. Rev. B **50**, 10893 (1994).
[19]X. Cartoixà, D. Z.-Y. Ting, and T. C. McGill, J. Appl. Phys. **93**, 3974 (2003).
[20]W. Yang and K. Chang, Phys. Rev. B **72**, 233309 (2005).
[21]T. Eissfeller and P. Vogl, Phys. Rev. B **84**, 195122 (2011).
[22]B. A. Foreman, Phys. Rev. B **56**, R12748 (1997).
[23]B. A. Foreman, Phys. Rev. B **75**, 235331 (2007).
[24]R. G. Veprek, S. Steiger, and B. Witzigmann, Phys. Rev. B **76**, 165320 (2007).
[25]A. V. Rodina, A. Yu. Alekseev, Al. L. Efros, M. Rosen, and B. K. Meyer, Phys. Rev. B **65**, 125302 (2002).
[26]Q. Zhao, T. Mei, and D. Hua Zhang, J. Appl. Phys. **111**, 053702 (2012).
[27]O. Stier and D. Bimberg, Phys. Rev. B **55**, 7726 (1997).
[28]J. D. Cooper, A. Valavanis, Z. Ikonić, P. Harrison, and J. E. Cunningham, J. Appl. Phys. **108**, 113109 (2010).
[29]I.-H. Tan, G. L. Snider, L. D. Chang, and E. L. Hu, J. Appl. Phys. **68**, 4071 (1990).
[30]H.-B. Wu, S. J. Xu, and J. Wang, Phys. Rev. B **74**, 205329 (2006).
[31]B. A. Foreman, Phys. Rev. Lett. **80**, 3823 (1998).
[32]B. A. Foreman, Phys. Rev. B **48**, 4964 (1993).
[33]P. C. Klipstein, Phys. Rev. B **81**, 235314 (2010).
[34]E. P. Pokatilov, V. A. Fonoberov, V. M. Fomin, and J. T. Devreese, Phys. Rev. B **64**, 245328 (2001).
[35]T. Mei, J. Appl. Phys. **102**, 053708 (2007).
[36]H. Jiang and J. Singh, Phys. Rev. B **56**, 4696 (1997).